

# RoboDuet: Whole-body Legged Loco-Manipulation with Cross-Embodiment Deployment

Guoping Pan, Qingwei Ben, Zhecheng Yuan, Guangqi Jiang, Yandong Ji,  
Shoujie Li, Jiangmiao Pang, Houde Liu, *Member, IEEE*, Huazhe Xu

**Abstract**—Fully leveraging the mobile manipulation capabilities of a quadruped robot equipped with a robotic arm is non-trivial, as it requires controlling all degrees of freedom (DoFs) of the quadruped robot to achieve effective whole-body coordination. In this letter, we propose a novel framework RoboDuet, which employs two collaborative policies to realize locomotion and manipulation simultaneously, achieving whole-body control through mutual interactions. Beyond enabling large-range 6D pose tracking for manipulation, we find that the two-policy framework supports cross-embodiment deployment, allowing for the use of different quadruped robots or various robotic arms. Our experiments demonstrate that RoboDuet achieves a 42.5% improvement in average success rate over the baseline in mobile manipulation tasks employing whole-body control. These policies also enable zero-shot deployment across different quadruped robots in the real world. To support further research, we provide open-source code and additional videos on our website: [locomanip-duet.github.io](https://locomanip-duet.github.io).

**Index Terms**—Legged robot, whole-body control, mobile manipulation, cross-embodiment, reinforcement learning.

## I. INTRODUCTION

Mobile robots have increasingly been deployed to assist humans and demonstrated remarkable capabilities [1], [2]. Typically, these robots are equipped with wheeled mobile bases, making them less adaptable to diverse terrains and unable to adjust their base posture. This limitation has sparked interest in developing legged robots to undertake manipulation tasks, offering enhanced versatility and adaptability in diverse environments. By employing whole-body control in legged robots and robotic arms, it is possible to effectively overcome terrain constraints and significantly expand the manipulation workspace of the arms [3], [4], [5]. However, training a

This work was supported by Institute for Interdisciplinary Information Sciences, Tsinghua University, Shanghai Qi Zhi Institute and Shanghai Artificial Intelligence Laboratory. (Guoping Pan and Qingwei Ben are co-first authors.) (Corresponding author: Huazhe Xu.)

Guoping Pan, Qingwei Ben, Zhecheng Yuan and Shoujie Li are with Tsinghua University, Beijing 100084, China. (email: pgp23@mails.tsinghua.edu.cn, elgceben@gmail.com, yuanzc23@mails.tsinghua.edu.cn, lsj20@mails.tsinghua.edu.cn)

Guangqi Jiang and Yandong Ji are with University of San Diego, California 92093, USA. (email: ggjiang@ucsd.edu, ydji1024@gmail.com)

Jiangmiao Pang is with Shanghai Artificial Intelligence Laboratory, Shanghai 200032, China. (email: pangjiangmiao@gmail.com)

Houde Liu is with Tsinghua Shenzhen International Graduate School, Shenzhen 518055, China, and also with Jianghuai Advance Technology Center, Hefei 230000. (email: liu.hd@sz.tsinghua.edu.cn)

Huazhe Xu is with the Institute for Interdisciplinary Information Sciences, Tsinghua University, Beijing 100084, China, and also with Shanghai Qi Zhi Institute, Shanghai 200030, China, as well as with Shanghai Artificial Intelligence Laboratory, Shanghai 200032, China. (email: huazhe\_xu@mails.tsinghua.edu.cn)

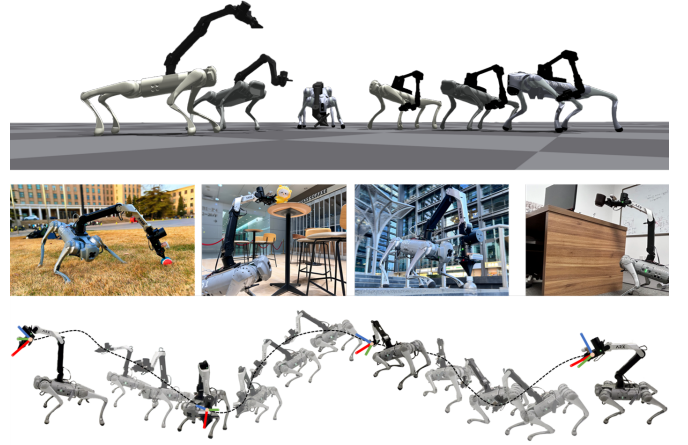


Fig. 1. RoboDuet is a framework that affords mobile-manipulation and cross-embodiment deployment. Top row: cross-embodiment deployment. This feature enables control across six configurations generated by the permutation of two robotic arms and three quadruped robots, allowing for component replacement without the need to retrain the entire system. Middle row: mobile manipulation. From left to right, the robot walks to pick up a small ball on grass, grasps a doll from a high table in a café, grabs a bottle on lower stairs, and picks up a cup from an office desk. Bottom row: whole-body control. Given multiple target end-effector poses, the robot can adjust its entire body posture while moving to reach the desired targets and maintain stability.

legged loco-manipulation robot to achieve whole-body control like humans, along with accurate pose tracking capabilities, presents a substantial challenge to researchers.

As a pioneering effort in this domain, Fu *et al.* [3] has utilized a unified control policy to accomplish coordinated manipulation and locomotion. Despite the implementation of a whole-body control framework, it cannot tackle accurate 6D end-effector pose tracking, a capability that is crucial for manipulation tasks. On the other hand, while GAMMA [4] and GeFF [5] are capable of grasping objects based on 6-DoF end-effector control, their operation strategies separate the arm and the quadruped systems, thus falling short of achieving whole-body control. This distinction restricts the workspace of the arm. Consequently, accomplishing large-range manipulation tasks across the entire workspace necessitates a novel training paradigm. This approach must ensure enhanced coordination between the quadruped and the manipulator arm while also improving training efficiency and generalization capabilities.

In awareness of these challenges, we introduce the **RoboDuet**: an integrated legged loco-manipulation framework tailored for large-range 6D pose tracking and whole-body control. As shown in Fig. 1, RoboDuet endows the policies with the capabilities of cross-embodiment deployment

across different quadruped robots and robotic arms, mobile manipulation for diverse tasks, and robust whole-body control. These capabilities greatly enhance the system's adaptability to different environments and reduce the need for retraining.

To simplify the whole-body control problem, we adopt a cooperative policy mechanism, achieved through the coordinated collaboration of a locomotion policy and an arm policy. The interaction between the locomotion policy and the arm's actions exhibits a duet-like performance, where the locomotion policy utilizes the actions of the arm as guidance to adjust its posture, while the arm is complemented by the actions of the locomotion policy aiming to expand the robot's workspace. The training process for RoboDuet is structured in two stages, as illustrated in Fig. 2. In stage 1, we develop the locomotion policy to endow the legged robot with essential mobility capabilities. Following stage 1, stage 2 involves training the arm policy that can coordinate with the locomotion policy. We argue that employing a two-stage training strategy enhances the stability of the training process, resulting in the acquisition of agile and large-range 6D pose tracking agents.

Our contributions are summarized as follows:

- We propose a framework that can simultaneously achieve robust locomotion and agile 6D end-effector pose tracking, thus capable of mobile manipulation.
- Our framework effectively coordinates the legged robot and the robotic arm with two collaborative yet separated policies, introducing the ability of whole-body control and cross-embodiment deployment.
- We conduct extensive simulation and real-world experiments to demonstrate the whole-body control, gait stability, and cross-embodiment ability of our framework.

## II. RELATED WORKS

### A. Learning-based Locomotion

Learning-based algorithms, especially deep reinforcement learning (DRL), have significantly advanced the locomotion of quadruped robots [6], [7], [8], [9]. In contrast to their control-based counterparts, which require extensive engineering for accurate physical modeling of dynamics [10], [11], learning-based algorithms rely primarily on straightforward reward functions to develop robust locomotion policies. Physics simulators represented by IsaacGym [12] enable efficient data sampling and the acquisition of privileged observations in simulations. Techniques such as RMA[13] and domain randomization have effectively reduced the sim2real gap. Currently, learning-based locomotion rivals its traditional model-based control counterparts in adaptability to navigate difficult terrains, climb stairs [14], [15], [16], and perform parkour [17], [18].

### B. Whole-body Control for Legged Robot

Given the superior locomotive capabilities of quadruped robots compared to chassis, there is an emerging interest in developing whole-body control for integrating legged robots and robotic arms to finish mobile manipulation tasks. The current technological landscape features three primary strategies. The first involves control-based techniques like model

predictive control (MPC), which require extensive engineering efforts and generally exhibit limited adaptability and robustness in complex environments [19], [20]. The second strategy adopts learning algorithms to generate high-level commands for legged robot or robotic arm, which are then translated into low-level joint control instructions based on built-in controllers or inverse kinematics (IK) [4], [5], [21], [22]. However, these approaches lack effective coordination between the legged platform and the arm or suffer from infeasible IK solutions, thus failing to maximize the potential for coordinating the pose of the legged robot to extend the operational range of the arm. The third approach leverages DRL to realize whole-body control. In earlier research, a unified policy is trained to control the entire system, achieving only end-effector position tracking [3]. A follow-up study extends this approach to 6D task-space pose tracking [23], but it is limited by the constraints of data collection. The most recent research leverages keypoint tracking to train a whole-body end-effector pose tracking policy, which requires an additional policy to provide locomotion capabilities [24]. Consequently, there is a clear need for innovative frameworks that are capable of harnessing the full locomotive advantages of quadruped robots while ensuring seamless coordination between the upper arm and the lower legged platform.

## III. METHODS

### A. Cooperative Policy for Whole-body Control

RoboDuet consists of a loco policy for locomotion and an arm policy for manipulation. The two policies are harmonized as a whole-body controller. Specifically, the loco policy adjusts its actions accordingly by following instructions from the arm policy. For each policy, we implement reinforcement learning algorithms to maximize the discounted expected return  $\mathbb{E}_{\pi_\theta} \left[ \sum_{t=0}^{T-1} \gamma^t r_t \right]$  to find the optimal parameters  $\theta$ , where  $r_t$  represents the reward at time step  $t$ ,  $\gamma$  is the discount factor, and  $T$  is the maximum episode length. We utilize the Proximal Policy Optimization (PPO) [25] algorithm for training.

1) **Loco policy:** The goal of the loco policy  $\pi_{loco}$  is to follow a target command  $\mathbf{c}_t = (v_x^{\text{cmd}}, v_y^{\text{cmd}}, \omega_{yaw}^{\text{cmd}}, \phi_{pitch}^{\text{cmd}}, \phi_{roll}^{\text{cmd}})$ , where  $v_{x,y}^{\text{cmd}} = (v_x^{\text{cmd}}, v_y^{\text{cmd}})$  are the desired linear velocity in base frame along x- and y- axes,  $\omega_{yaw}^{\text{cmd}}$  is the desired angular velocity in yaw axis,  $\phi^{\text{cmd}} = (\phi_{pitch}^{\text{cmd}}, \phi_{roll}^{\text{cmd}})$  denotes the desired pitch and roll angle of the base which plays an important role in achieving whole-body control and many downstream tasks. The observation of loco policy  $\mathbf{o}_t^{\text{loco}}$  contains leg states  $\mathbf{s}_t^{\text{leg}} \in \mathbb{R}^{26}$  (leg joint positions and velocities), base states  $\phi_t$  (roll and pitch angles), target commands  $\mathbf{c}_t$ , clock time  $\mathbf{t}_t$ , and last leg action  $\mathbf{a}_{t-1}^{\text{leg}} \in \mathbb{R}^{12}$ . The leg action  $\mathbf{a}_t^{\text{leg}}$  represents a joint position offset that is added to the default joint position to specify the target position for twelve leg joint motors.

2) **Arm policy:** The goal of the arm policy  $\pi_{arm}$  is to accurately track the 6D pose. The observations of arm policy  $\mathbf{o}_t^{\text{arm}}$  is composed of arm states  $\mathbf{s}_t^{\text{arm}} \in \mathbb{R}^{12}$  (arm joint positions and velocities), target end-effector pose  $\chi_t \in \mathbb{R}^6$ , base states  $\phi_t$ , and last arm action  $\mathbf{a}_{t-1}^{\text{arm}} \in \mathbb{R}^8$ . The actions of the arm policy consist of two parts: the first six actions  $\mathbf{a}_t^{\text{arm}^J} \in \mathbb{R}^6$  represent the target joint position offsets corresponding to six arm joint

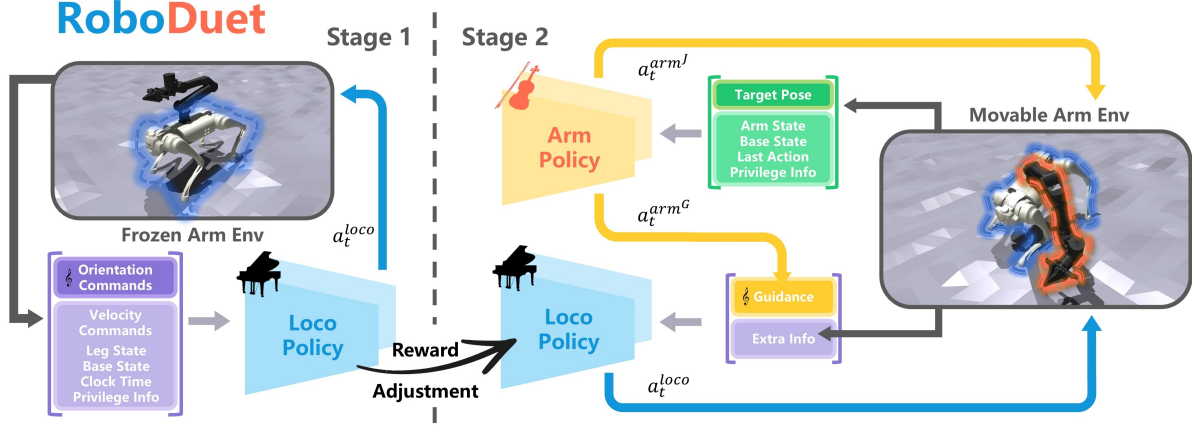


Fig. 2. Overview of the framework. RoboDuet operates in two stages. In Stage 1, the loco policy is trained with the robotic arm fixed, enabling the quadruped robot to achieve robust locomotion. In Stage 2, the loco and arm policies are trained simultaneously in a cooperative manner. The loco policy from stage 1 is reused, but the original body orientation commands are replaced by guidance signals  $a_t^{arm^G}$  generated by the arm policy, enabling coordinated whole-body control. During the transition between the two stages, reward adjustment is introduced to effectively leverage locomotion priors, facilitating seamless integration for whole-body mobile manipulation.

actuators. Then, it will be concatenated with the output of the loco policy to achieve synchronous control of the overall system. It should be mentioned that the position targets are tracked using a proportional-derivative controller. To expand the manipulation workspace with whole-body control, the rest part of the arm policy  $a_t^{arm^G} = (a_t^{arm^p}, a_t^{arm^r}) \in \mathbb{R}^2$  is used to replace  $\phi^{cmd}$ , providing additional degrees of freedom for end-effector tracking to cooperate with the loco policy. Due to the distinct focuses of the two policies, only essential information is shared to maintain a favorable cooperative relationship while mitigating disruptions caused by factors such as differences in task learning efficiency.

### B. Two-stage Training

To ensure robust mobile manipulation, we employ a two-stage training strategy. Our method enables a seamless transition between these stages by maintaining consistent input and output dimensions for the policies throughout the entire process. Since the primary tasks differ across the stages—stage 1 focuses on locomotion, while stage 2 emphasizes manipulation—we introduce reward adjustment to integrate the latter without compromising the performance of the former.

1) **Stage 1:** This stage focuses on obtaining the robust locomotion capability. To ensure that the loco policy adapt to the center of mass and the inertia offset of the whole robot throughout the entire training process, we keep all the arm joints fixed at their default positions  $[0, 0.8, 0.8, 0, 0, 0]$ . In this stage, the arm policy is inactive, and the target end-effector pose  $\chi_t$  is set to zero. Inspired by the powerful blind locomotion algorithm [16], we similarly apply a vector of behavior parameters  $\mathbf{b}_t$  to represent a heuristic gait reward, which is expressed as follows:

$$\mathbf{b}_t = [\theta_1^{cmd}, \theta_2^{cmd}, \theta_3^{cmd}, f^{cmd}, h_z^{cmd}, \phi^{cmd}, s^{cmd}, h_z^{f,cmd}] \quad (1)$$

where  $\theta^{cmd} = (\theta_1^{cmd}, \theta_2^{cmd}, \theta_3^{cmd})$  are the timing offsets between pairs of feet. Since our goal is to achieve pose

tracking rather than diverse locomotion behaviors, we fix some gait parameters to speed up the convergence of training. In the following description, we specifically highlight the modified parts. We set the timing offsets  $\theta^{cmd}$  to  $[0.5, 0, 0]$  to achieve a stable trotting gait. To enable the loco policy to recognize the rhythm of stepping, the clock time  $t_t$  is computed from the offset timings of each foot, with the mathematical definitions as follows:

$$\begin{aligned} t_t &= [\sin(2\pi t^{FR}), \sin(2\pi t^{FL}), \sin(2\pi t^{RR}), \sin(2\pi t^{RL})] \quad (2) \\ [t^{FR}, t^{FL}, t^{RR}, t^{RL}] &= [t + \theta_2^{cmd} + \theta_3^{cmd}, t + \theta_1^{cmd} + \theta_3^{cmd}, \\ &\quad t + \theta_1^{cmd}, t + \theta_2^{cmd}] \quad (3) \end{aligned}$$

where  $t$  is a counter variable that advances from 0 to 1 during each gait cycle and FR, FL, RR, RL are the four feet respectively. When the base velocity is zero, the jitter caused by marching on the spot will reduce the precision of manipulation. In this situation, we set clock time  $t_t$  to  $[1, 1, 1, 1]$  to force all feet to maintain a stationary position.  $f^{cmd}$  is the stepping frequency which is set to 3 Hz.  $h_z^{cmd}$  is the body height command which is not used.  $s^{cmd} = (s_x^{cmd}, s_y^{cmd})$  is the foot clearance which is set to  $[0.45, 0.3]$ .  $h_z^{f,cmd}$  is the footswing height command which is set to 0.06 m.

During stage one, most components of the reward  $r^{loco}$  utilized by the loco policy are identical to those described in [16], which can be referred to for more details. However, we remove the body height tracking component  $r_{h_z^{cmd}}^{loco}$  to allow the body height to adjust adaptively according to the task. Due to the additional payload introduced by the arm, we incorporate an energy reward  $r_{energy}^{loco}$  for the quadruped robot to facilitate smoother motion [26], as formulated below:

$$r_{energy}^{loco} = -0.00004 \cdot \sum_{i \in \text{leg joints}} |\tau_i \dot{q}_i|^2 \quad (4)$$

where  $\tau_i$  and  $\dot{q}_i$  is the torque and velocity of the  $i^{th}$  leg joint.

2) **Stage 2:** This stage aims to coordinate locomotion and manipulation to achieve whole-body large-range mobile manipulation. The arm policy is activated simultaneously with all the robotic arm joints. We adopt 6D target pose of end-effector as policy input. To eliminate the influence brought by body rotation [3], we similarly use a posture-independent spherical coordinate to define the target end-effector pose  $\chi_t$ . The target position of end-effector is represented by radius  $l$ , latitude  $p$ , and longitude  $y$ . To improve the accuracy of end-effector orientation tracking, we use euler angles  $[roll, pitch, yaw]$  in Z-Y-X order for sampling, which can intuitively exclude many illegal postures, and convert them to included angle along each axis of the coordinate. The mathematical form of sampling can be expressed as follows:

$$R = R_{yaw} \cdot R_{pitch} \cdot R_{roll} = \begin{bmatrix} r_{11} & r_{12} & r_{13} \\ r_{21} & r_{22} & r_{23} \\ r_{31} & r_{32} & r_{33} \end{bmatrix} \quad (5)$$

$$[\alpha, \beta, \gamma] = [\tan^{-1}(\frac{r_{21}}{r_{11}}), \tan^{-1}(\frac{r_{32}}{r_{22}}), \tan^{-1}(\frac{r_{13}}{r_{33}})] \quad (6)$$

Here,  $R$  is the composite rotation obtained by sequentially rotating around the z-axis, y-axis, and x-axis.  $\gamma, \beta, \alpha$  represent the included angles with corresponding axes. To simultaneously minimize both position and orientation errors of the end-effector, the target pose tracking reward  $r_{\chi_t}$  is constructed in exponential form:

$$r_{\chi_t} = e^{-w \cdot \Delta(l, p, y)} \cdot e^{-\Delta(\alpha, \beta, \gamma)} \quad (7)$$

$$\begin{cases} \Delta(l, p, y) = \sum_{u \in (l, p, y)} k_u \cdot |u_t - u^{\text{cmd}}| \\ \Delta(\alpha, \beta, \gamma) = \sum_{u \in (\alpha, \beta, \gamma)} k_u \cdot |u_t - u^{\text{cmd}}| \end{cases} \quad (8)$$

where weight coefficient  $w$  is used to balance the priority of the two components. The function  $\Delta(\cdot)$  is defined as the sum of absolute errors between each variable and its respective target value within the set, and  $k_i$  represents the reciprocal of the sampling range for each variable, which is used to rescale the errors. The target pose tracking reward  $r_{\chi_t}$  is utilized for both the loco and arm policies in stage 2.

TABLE I  
KEY REWARD TERMS, EQUATION, AND  
WEIGHTS USED IN STAGE 1 AND STAGE 2

Term	Equation	Weight	
		stage 1	stage 2
$r_{\text{loco}}^{\text{cmd}}$	$(\mathbf{p}_{x,y,\text{foot}}^f - \mathbf{p}_{x,y,\text{foot}}^{f,\text{cmd}} (s^{\text{cmd}}))^2$	-10.0	0.0
$r_{\text{hip}}^{\text{loco}}$	$\sum_{\text{hip}}  a_t ^2$	0.0	-0.05
$r_{v_{x,y}}^{\text{cmd}}$	$\exp\left\{- v_{x,y} - v_{x,y}^{\text{cmd}} ^2 / \sigma_{v_{x,y}}\right\}$	1.0	0.5
$r_{\omega_{yaw}}^{\text{cmd}}$	$\exp\left\{-(\omega_{yaw} - \omega_{yaw}^{\text{cmd}})^2 / \sigma_{\omega_{yaw}}\right\}$	0.5	0.25
$r_{\text{smooth}}^{\text{arm}}$	$ a_{t-1}^{\text{arm}} - a_t^{\text{arm}} ^2$	0.0	-0.1
$r_{\text{guide}}^{\text{arm}}$	$ \phi_t - a_t^{\text{arm}G} $	0.0	-10.0

3) **Reward Adjustment:** While the rewards in stage 1 drive the quadruped robot to achieve robust locomotion, the fixed foot placements are not conducive to the whole-body control required in stage 2, when the robot needs to adapt its body posture by altering foot placements. To address this, the raibert heuristic footswing tracking reward  $r_{\text{cmd}}^{\text{loco}}$  is replaced by the hip joint constraint reward  $r_{\text{hip}}^{\text{loco}}$ . Additionally, the velocity tracking reward  $r_{v_{x,y}}^{\text{cmd}}, r_{\omega_{yaw}}^{\text{cmd}}$  is scaled to half its original value to accommodate different tasks. The reward adjustments are detailed in Table I. To achieve more coordinated whole-body control, we introduce  $r_{\text{smooth}}^{\text{arm}}$  and  $r_{\text{guide}}^{\text{arm}}$  to promote smoother arm motion and enhance the control of the body orientation.

## IV. EXPERIMENT DESIGN

### A. Robot System

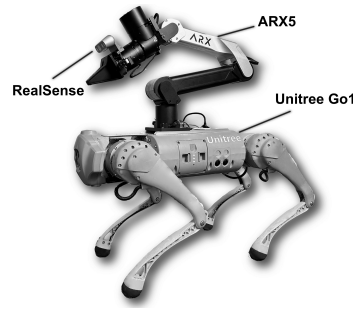


Fig. 3. The robot system, consisting of a quadruped robot (Unitree Go1 Edu) with a mounted robotic arm (ARX5) and a camera (RealSense D435i).

The robot system used in our experiments consists of a 12-DoF legged robot Unitree Go1 Edu and a 6-DoF robotic arm ARX5 with a parallel gripper, as shown in Fig. 3. The Go1 weighs 12 kg, and the ARX5, mounted on its back, weighs 3.35 kg. A RealSense D435i camera is positioned above the gripper to maintain a fixed relative pose. The ARX5 offers a rated load capacity of 1.5 kg and a maximum reach

of 620 mm. The control frequency is set to 50 Hz for both training and deployment.

### B. Algorithm Comparison

In order to examine the performance of our proposed method on whole-body control, 6D pose tracking, cross-embodiment, and mobile manipulation, we set up comparisons of the following algorithms:

- **Floating Base+IK:** A floating base policy without whole-body control for the quadruped robot, combined with an IK solver [27] for arm.
- **Unified:** A unified policy with two output heads corresponding to the control of quadruped robot and arm. Training starts directly from stage 2.
- **Two-Stage:** The same policy settings as the Unified are used, but with a two-stage training approach.
- **Cooperated:** This setting uses the cooperative policy. Training starts directly from stage 2.
- **RoboDuet:** The same policy settings as the Cooperated are used, but with a two-stage training approach.

The first setting serves as a baseline to evaluate the solution stability of our method. The primary distinctions among the remaining four settings lie in whether they use a cooperative policy and a two-stage training approach, which are the two key components of our method. This comparison allows us to assess the effectiveness of each component.

### C. Training Details

We train 4096 parallel agents using the IsaacGym simulator [12]. We train all algorithms for 50,000 iterations across 3 seeds, with the two-stage training comprising 10,000 iterations for stage 1 and 40,000 for stage 2, employing the asymmetric actor-critic framework used in [28]. All neural networks are designed as the Multilayer Perceptron (MLP) with ELU [29] activations for hidden layers. Unlike the cooperative policy, the unified policy merges feature extractors into one, so we double the number of neurons in the hidden layers. All training is performed on NVIDIA RTX 4090 GPUs.

### D. Sample space

The sample ranges utilized for both training and evaluation are detailed in Table II. The evaluation sample space is slightly larger than the training one to demonstrate the generalization of algorithms, which already covers all 6D poses in the front hemisphere space. During the evaluation, we uniformly sample 200,000 target commands at random from the ranges to facilitate a comparative analysis of various algorithms.

TABLE II  
RANGES OF COMMANDS USED IN TRAINING AND EVALUATION

Parameter	Range	
	Training	Evaluation
$v_x$ (m/s)	[-1.00, 1.00]	[-1.50, 1.50]
$\omega_z$ (rad/s)	[-0.60, 0.60]	[-1.00, 1.00]
$l$ (m)	[0.30, 0.70]	[0.20, 0.80]
$p$ (rad)	[-0.45 $\pi$ , 0.45 $\pi$ ]	[-0.50 $\pi$ , 0.50 $\pi$ ]
$y$ (rad)	[-0.50 $\pi$ , 0.50 $\pi$ ]	[-0.50 $\pi$ , 0.50 $\pi$ ]
$\alpha$ (rad)	[-0.45 $\pi$ , 0.45 $\pi$ ]	[-0.50 $\pi$ , 0.50 $\pi$ ]
$\beta$ (rad)	[-0.33 $\pi$ , 0.33 $\pi$ ]	[-0.50 $\pi$ , 0.50 $\pi$ ]
$\gamma$ (rad)	[-0.42 $\pi$ , 0.42 $\pi$ ]	[-0.50 $\pi$ , 0.50 $\pi$ ]

### E. Metrics

To quantify the performance of the algorithm, we define several metrics: (1) velocity tracking error, measured by the difference between the target commands and actual states for  $v_x$ ,  $v_y$ , and  $\omega_{yaw}$ ; (2) position tracking error, determined by the error for  $l$ ,  $p$ ,  $y$ , and the Euclidean distance  $D$ ; (3) orientation tracking error, calculated based on the angles  $\alpha$ ,  $\beta$ ,  $\gamma$ , and the quaternion geodesic distance  $\zeta$ ; (4) survival rate, assessed by randomly applying forces of 10 to 20 newtons to the base for 2 seconds and calculating the proportion of robots that maintain a base height above 0.26 m across all samples; (5) solvability, defined as the ratio of collision-free poses to the total number of samples; and (6) workspace, defined as the area of the convex hull formed by all target commands within the tracking error threshold, ensuring no self-collisions throughout the tracking process. A sample is considered successful if the tracking of the end-effector pose meets the thresholds of  $D \leq 0.03$  m for distance and  $\theta \leq \pi/36$  for orientation, where  $\theta$  is the angle between the two vectors obtained by applying the target orientation and end-effector orientation to the same unit vector. The maximum time allowed to reach the target

command is 4 seconds, after which the average error over the following 2 seconds is computed.

## V. RESULTS

### A. Simulation Experiments

1) *Ablation*: To validate the significance of the two-stage training and the cooperative policy mechanism, which are key components of RoboDuet, we conduct sufficient ablation experiments by comparing with Unified, Two-Stage and Co-operated. The results are shown in Table III, which demonstrate that all configurations meet the requirements for stable standing. Although two-stage training does not significantly improve end-effector pose tracking, it demonstrates a notable improvement in resisting external perturbations. Specifically, Two-Stage improves survival rates by 10.93% over the Unified, attributed to the focus of stage 1 on optimizing locomotion. On the other hand, Cooperated and RoboDuet outperform both the Unified and Two-Stage configurations across almost all metrics, indicating that the cooperative policy mechanism effectively decouples multi-task learning, enabling the two policies to collaborate while maintaining focus. Cooperated achieves the best performance in velocity tracking and position tracking, largely due to its lack of the gait prior constraint from stage 1, allowing it to take a more aggressive approach in achieving higher tracking rewards which results a decrease on survival rates. In comparison, RoboDuet maintains comparable end-effector tracking performance while achieving robust locomotion motion ability and offers a larger operational workspace during motion. In summary, by effectively integrating cooperative policy and two-stage training, RoboDuet significantly enhances control performance in both tracking accuracy and gait stability, underscoring the essential role of these components.

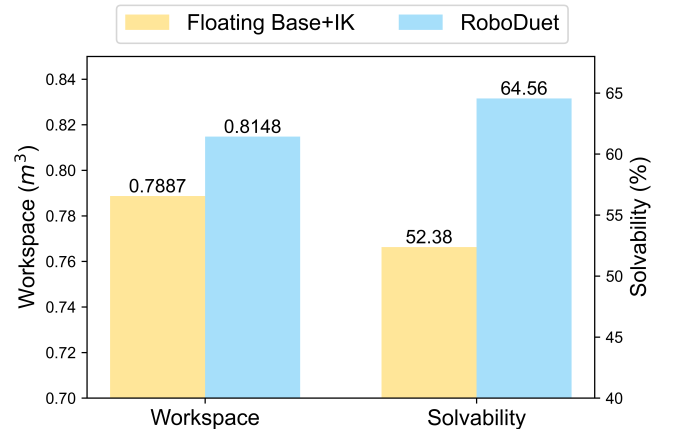


Fig. 4. Comparison of Solvability and Workspace between Floating Base+IK and RoboDuet.

2) *Whole-body Control*: To validate the effectiveness of our proposed whole-body control training framework RoboDuet, we make a comparison with the Floating Base+IK. To be fair, we evaluate the solvability and workspace under the same error threshold by applying the average Euclidean distance error and quaternion geodesic distance error of RoboDuet as the pose error thresholds for IK solver. For both, the initial



TABLE III  
ABLATION RESULTS OF DIFFERENT METHODS IN STILL AND MOVE MODES  
"STILL" MEANS ALL VELOCITY COMMANDS ARE ZERO, WHILE "MOVE" INVOLVES RANDOM VELOCITY SAMPLING DURING EVALUATION.

Metrics (scaled by $10^{-2}$ )		Still				Move			
		Baseline	Two-Stage	Cooperative	RoboDuet	Baseline	Two-Stage	Cooperative	RoboDuet
Velocity Tracking ↓	$v_x$ (m/s)	0.47±0.00	0.48±0.00	0.34±0.00	<b>0.32±0.00</b>	13.58±0.00	14.00±0.02	<b>10.12±0.00</b>	12.12±0.00
	$v_y$ (m/s)	0.40±0.00	0.47±0.00	0.39±0.00	<b>0.37±0.00</b>	20.12±0.01	18.57±0.05	<b>15.87±0.00</b>	16.51±0.00
	$\omega_z$ (rad/s)	0.32±0.00	0.34±0.00	0.32±0.00	<b>0.32±0.00</b>	62.58±0.00	62.76±0.00	<b>60.67±0.00</b>	60.95±0.00
Position Tracking ↓	$l$ (m)	4.23±0.00	3.82±0.00	<b>2.58±0.00</b>	2.59±0.00	4.05±0.00	3.65±0.00	2.59±0.00	<b>2.45±0.00</b>
	$p$ (rad)	26.07±0.07	23.78±0.23	<b>19.33±0.04</b>	20.98±0.03	22.06±0.02	21.08±0.14	<b>18.85±0.04</b>	19.89±0.02
	$y$ (rad)	19.46±0.04	17.71±0.03	11.63±0.00	<b>10.97±0.00</b>	18.73±0.04	15.56±0.01	11.62±0.00	<b>10.72±0.00</b>
	$D$ (m)	16.21±0.01	15.00±0.04	<b>12.17±0.01</b>	12.87±0.01	14.50±0.00	13.46±0.02	<b>12.05±0.01</b>	12.26±0.00
Orientation Tracking ↓	$\alpha$ (rad)	43.60±0.07	46.77±0.09	<b>42.72±0.11</b>	43.33±0.02	44.05±0.11	46.34±0.04	<b>42.40±0.12</b>	43.12±0.02
	$\beta$ (rad)	59.17±0.02	60.72±0.04	49.79±0.06	<b>46.66±0.04</b>	56.13±0.03	61.34±0.23	49.52±0.05	<b>47.43±0.05</b>
	$\gamma$ (rad)	51.95±0.03	52.70±0.06	40.74±0.03	<b>40.15±0.02</b>	52.20±0.04	54.67±0.07	42.00±0.03	<b>41.82±0.00</b>
	$\zeta$ (-)	50.87±0.00	52.17±0.00	48.10±0.00	<b>48.07±0.00</b>	50.62±0.00	52.25±0.01	48.16±0.00	<b>48.10±0.02</b>
Survival Rate (%) ↑		84.46±0.92	95.39±0.03	93.80±0.07	<b>96.60±0.01</b>	92.83±1.58	99.50±0.00	99.37±0.00	<b>99.91±0.00</b>
Workspace ( $m^3$ ) ↑		42.40±0.23	51.22±0.32	<b>82.47±0.02</b>	81.89±0.04	73.55±0.02	73.78±0.07	84.77±0.00	<b>85.18±0.01</b>

joint positions of the arm are set to the same as default positions mentioned in Section III-B1. According to Fig. 4, RoboDuet demonstrates a 12.18% improvement in solvability compared to the Floating Base+IK configuration. Furthermore, the workspace comparison suggests that whole-body control can significantly enhance the operational capabilities of the robotic arm. It is worth reiterating that solvability is defined as reaching the target pose from the current pose without any collisions throughout the entire process. Additionally, many samples are inherently unreachable due to the limitations imposed by the structure of the robotic arm itself.

TABLE IV  
WORKSPACE AND SURVIVAL RATE OF COMBINING THE ARX5 WITH DIFFERENT LEGGED ROBOTS

X+ARX	Workspace ( $m^3$ )		Survival Rate (%)	
	Still	Move	Still	Move
Go1	0.8189	0.8518	96.60	99.91
Go2	0.8150	0.8019	96.56	91.69
A1	0.8305	0.7957	99.37	91.72

3) *Cross-Embodiment*: To exhibit the cross-embodiment capability of RoboDuet, we select two additional quadruped robots Unitree A1 and Unitree Go2. We mount the ARX5 on these quadruped robots and train the system using the same method as in stage 1. After convergence, we obtain specific loco policies for the new embodiments. We evaluate the workspaces and survival rates under external forces by directly combining the previously trained arm policy for the Go1+ARX5 with newly developed locomotion policies. As shown in Table IV, even without additional training in stage 2, the newly integrated systems Go2+ARX and A1+ARX maintain relatively robust locomotion and accurate pose tracking, closely matching the performance of the original Go1+ARX system. This outcome underscores the exceptional zero-shot cross-embodiment capability of RoboDuet. Notably, under still

conditions, A1+ARX achieves an even higher survival rate of 99.37% along with a larger workspace of 0.8305. Due to fundamental differences among the various embodiments, only Go1+ARX5 demonstrates an increase in stability and an expansion of workspace during motion through its custom-tailored cooperative policy. In contrast, the other two systems exhibit slight decreases in performance. Nevertheless, they still achieve a survival rate of nearly 91% under external perturbations.

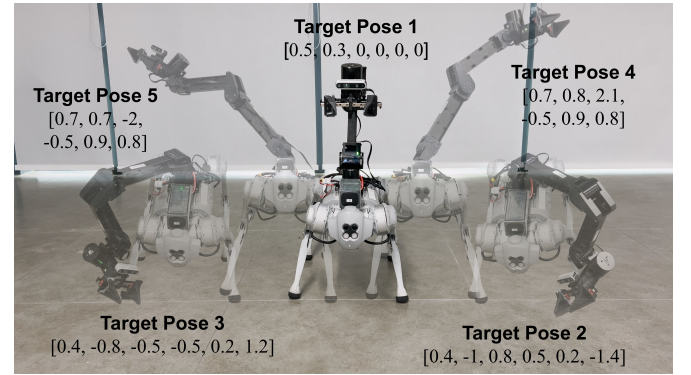


Fig. 5. Tracking extreme 6D poses with RoboDuet. The target pose is represented as  $[l, p, y, \text{roll}, \text{pitch}, \text{yaw}]$ , with  $l$  in meters and the others in radians. For certain unreachable targets, RoboDuet achieves stable approximations to optimal solutions.

## B. Real-world Experiments

In terms of real-world experiments, we craft three distinct types of tasks to validate the effectiveness of our policy in the real world and its proficiency in handling diverse mobile manipulation challenges. We directly deploy Floating Base+IK and RobotDuet on a real-world robotic system for testing.

1) *Extreme 6D Pose Tracking*: To evaluate the robustness and generalization of end-effector pose tracking, we select five

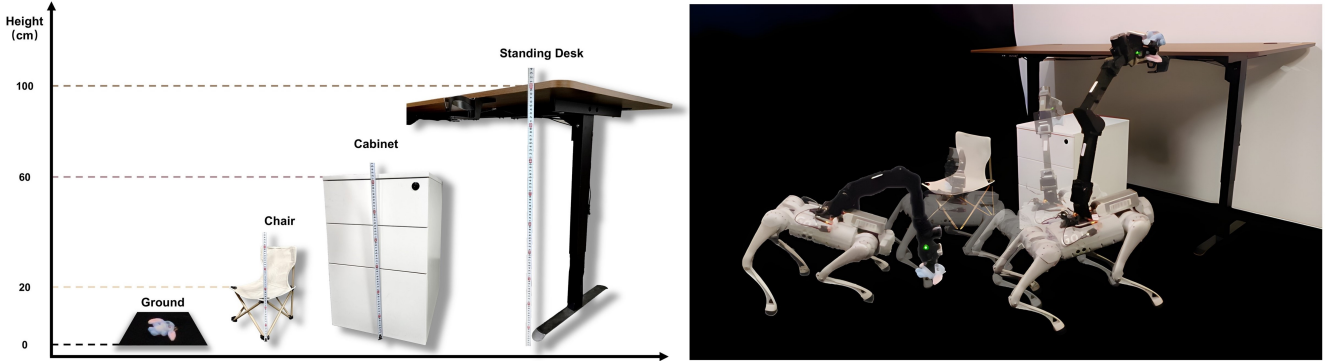


Fig. 6. Transferring objects between different heights, including the ground (0 cm), a camping chair (20 cm), a cabinet (60 cm), and the cup holder of a standing desk (100 cm). The right part illustrates how RoboDuet utilizes whole-body control to adapt its posture for varying grasp poses during transfer tasks.

target poses to evaluate their self-collision and solvability. The target poses are illustrated in Fig. 5, with four representing extreme 6D target configurations. Poses 2 and 3 are close to the ground and intersect with the robot’s legs, while poses 4 and 5 are significantly elevated above the robot, beyond the training sampling range. Notably, pose 5 is located on the right side, nearing the robotic arm’s maximum reach, and oriented towards the robot’s head, representing an highly pathological configuration that is unsolvable. For each pose, we conduct eight repetitions, and the results are shown in Table V. The IK system fails to resolve poses 2, 4, and 5. However, RoboDuet maintains stability across all poses and approached optimal approximate solutions for physically unreachable poses. Although pose 3 can be solved using IK, the floating base policy lacks whole-body control, leading to self-collision issues. Additionally, as training did not include the situation that arm in motion, tracking during poses 4 and 5 results in a higher risk of tipping, which we regard as self-collision. Due to the self-collision penalty integrated into the training process and its ability to maintain locomotion while the arm is in motion, RoboDuet experiences no collisions in nearly 95% of trials, with the arm stopping effectively near the legs in poses 2 and 3.

TABLE V  
SELF-COLLISION AND IK FAILURE RATE OF  
FLOATING BASE + IK VS. ROBODUET

Method	Self-collision Rate	IK Failure Rate
Floating Base+IK	50%	60%
RoboDuet	5%	-

2) *Whole-body Control*: To further analyze the impact of whole-body control on mobile manipulation, we design a set of tasks involving transferring a doll from varying heights, as shown in Fig. 6. For each height, we perform 10 repeated trials. A trial is considered successful only if the object is picked up and transferred to the next height without being dropped at any moment during this process. The system’s speed is controlled via a joystick on the remote controller, while the end-effector of the robotic arm is operated through a VR device. The experimental results are shown in Table VI.

TABLE VI  
SUCCESS RATE OF FLOATING BASE + IK VS. ROBODUET  
DURING THE TRANSFER OF OBJECTS BETWEEN DIFFERENT HEIGHTS

Method	Change in Height (cm)				Avg
	0 → 20	20 → 60	60 → 100	100 → 0	
Floating Base+IK	20%	40%	0%	0%	15.0%
RoboDuet	60%	80%	40%	50%	57.5%

When grasping objects on the ground, it is crucial to avoid both self-collisions and collisions with the ground. Lacking whole-body control capabilities, the Floating Base+IK approach is prone to self-collisions and failure, particularly when picking up objects positioned in front of or below the head. In contrast, RoboDuet can adjust its body posture to minimize collisions during grasping, resulting in a 40% increase in success rate. As the height increases, the need for body posture adjustments decreases, resulting in a 20% improvement in success rates for both approaches. Placing or retrieving the doll from the cup holder on a standing desk presented a particularly challenging task. The robotic arm was required to maintain a horizontal or top-down pose while operating near its maximum reach, when IK often fails to find a valid solution. RoboDuet demonstrates high solution stability and was able to reduce the vertical distance between the base and the standing desk by inclining its body, which successfully completed approximately 50% of the trials. In summary, across the complete object transfer process, RoboDuet achieved an average success rate of 57.5%, representing a 42.5% improvement over the Floating Base+IK.

3) *Cross-Embodiment*: To evaluate the generalizability of our method across different robot embodiments, we directly deploy the policy trained on the Unitree Go1+ARX5 to the Unitree Go2+ARX5. The Unitree Go1 weighs 12 kg, while the Unitree Go2 weighs 18 kg, representing a 41.6% increase in mass. Despite the significant increase in mass, RoboDuet still demonstrated robust whole-body control across both platforms, as illustrated in Fig. 7. The figure depicts four key moments of the two systems tracking the same trajectory, demonstrating consistent 6D pose tracking and robust whole-body control capabilities across both configurations.

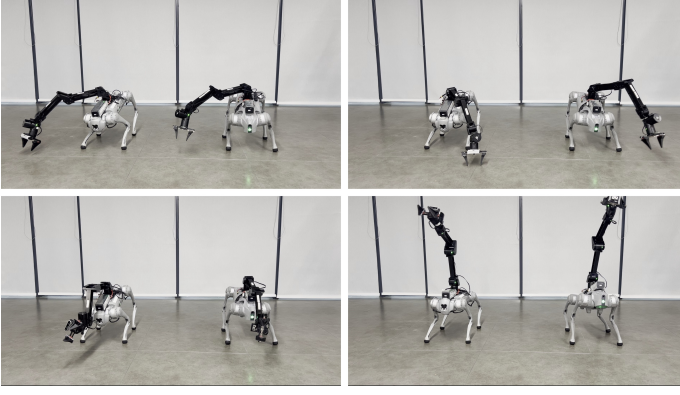


Fig. 7. Zero-shot deployment of RoboDuet, trained on the Unitree Go1+ARX5 (left), onto the Unitree Go2+ARX5 (right). The bottom-left image illustrates consistent agile 6D pose tracking, while the others highlight coordinated whole-body control.

## VI. DISCUSSION AND LIMITATIONS

In this letter, we propose RoboDuet, a whole-body mobile manipulation framework that integrates two collaborative policies for velocity tracking and 6D end-effector pose control, enabling agile and robust performance across diverse tasks. Leveraging a two-stage training approach, RoboDuet effectively utilizes robust locomotion priors to enhance the system’s resistance to external disturbances. Additionally, our method supports cross-embodiment deployment, allowing seamless hardware replacement without retraining, and it achieves real-world performance comparable to simulation.

While RoboDuet focuses on low-level whole-body control, achieving fully autonomous task execution will require integration with high-level planners and advanced collision detection. These are key areas for future enhancement.

## REFERENCES

- [1] Z. Fu, T. Z. Zhao, and C. Finn, “Mobile aloha: Learning bimanual mobile manipulation with low-cost whole-body teleoperation,” in *Conference on Robot Learning (CoRL)*, 2024.
- [2] J. Wu, R. Antonova, A. Kan, M. Lepert, A. Zeng, S. Song, J. Bohg, S. Rusinkiewicz, and T. Funkhouser, “Tidybot: Personalized robot assistance with large language models,” in *2023 IEEE/RSJ International Conference on Intelligent Robots and Systems (IROS)*. IEEE, 2023, pp. 3546–3553.
- [3] Z. Fu, X. Cheng, and D. Pathak, “Deep whole-body control: learning a unified policy for manipulation and locomotion,” in *2023 Conference on Robot Learning (CoRL)*. PMLR, 2023, pp. 138–149.
- [4] J. Zhang, N. Gireesh, J. Wang, X. Fang, C. Xu, W. Chen, L. Dai, and H. Wang, “Gamma: Graspability-aware mobile manipulation policy learning based on online grasping pose fusion,” in *2024 IEEE international conference on robotics and automation (ICRA)*. IEEE, 2024.
- [5] R.-Z. Qiu, Y. Hu, G. Yang, Y. Song, Y. Fu, J. Ye, J. Mu, R. Yang, N. Atanasov, S. Scherer *et al.*, “Learning generalizable feature fields for mobile manipulation,” *arXiv preprint arXiv:2403.07563*, 2024.
- [6] J. Long, Z. Wang, Q. Li, L. Cao, J. Gao, and J. Pang, “The him solution for legged locomotion: Minimal sensors, efficient learning, and substantial agility,” *2024 Proceedings of the International Conference on Learning Representations (ICLR)*, 2024.
- [7] A. Agarwal, A. Kumar, J. Malik, and D. Pathak, “Legged locomotion in challenging terrains using egocentric vision,” in *2022 Conference on robot learning (CoRL)*. PMLR, 2022, pp. 403–415.
- [8] Z. Fu, A. Kumar, A. Agarwal, H. Qi, J. Malik, and D. Pathak, “Coupling vision and proprioception for navigation of legged robots,” in *2022 Proceedings of the IEEE/CVF Conference on Computer Vision and Pattern Recognition (CVPR)*. IEEE, 2022, pp. 17 252–17 262.
- [9] K. Lei, Z. He, C. Lu, K. Hu, Y. Gao, and H. Xu, “Uni-o4: Unifying online and offline deep reinforcement learning with multi-step on-policy optimization,” *2024 Proceedings of the International Conference on Learning Representations (ICLR)*, 2024.
- [10] R. Grandia, F. Jenelten, S. Yang, F. Farshidian, and M. Hutter, “Perceptive locomotion through nonlinear model-predictive control,” *IEEE Transactions on Robotics (TRO)*, 2023.
- [11] N. Rathod, A. Bratta, M. Focchi, M. Zanon, O. Villarreal, C. Semini, and A. Bemporad, “Model predictive control with environment adaptation for legged locomotion,” *IEEE Access*, pp. 145 710–145 727, 2021.
- [12] V. Makovychuk, L. Wawrzyniak, Y. Guo, M. Lu, K. Storey, M. Macklin, D. Hoeller, N. Rudin, A. Allshire, A. Handa *et al.*, “Isaac gym: High performance gpu-based physics simulation for robot learning,” *2021 Proceedings of the Neural Information Processing Systems Track on Datasets and Benchmarks 1, NeurIPS Datasets and Benchmarks (NeurIPS)*, 2021.
- [13] A. Kumar, Z. Fu, D. Pathak, and J. Malik, “Rma: Rapid motor adaptation for legged robots,” *2021 Robotics: Science and Systems XVII (RSS)*, 2021.
- [14] R. Yang, G. Yang, and X. Wang, “Neural volumetric memory for visual locomotion control,” in *2023 Proceedings of the IEEE/CVF Conference on Computer Vision and Pattern Recognition (CVPR)*. IEEE, 2023, pp. 1430–1440.
- [15] G. B. Margolis, G. Yang, K. Paigwar, T. Chen, and P. Agrawal, “Rapid locomotion via reinforcement learning,” in *The International Journal of Robotics Research (IJRR)*, 2024, pp. 572–587.
- [16] G. B. Margolis and P. Agrawal, “Walk these ways: Tuning robot control for generalization with multiplicity of behavior,” in *2023 Conference on Robot Learning (CoRL)*. PMLR, 2023, pp. 22–31.
- [17] Z. Zhuang, Z. Fu, J. Wang, C. Atkeson, S. Schertfeger, C. Finn, and H. Zhao, “Robot parkour learning,” in *2023 Conference on Robot Learning (CoRL)*. PMLR, 2023, pp. 73–92.
- [18] X. Cheng, K. Shi, A. Agarwal, and D. Pathak, “Extreme parkour with legged robots,” in *2023 Conference on Robot Learning (CoRL)*. PMLR, 2023.
- [19] J.-P. Sleiman, F. Farshidian, and M. Hutter, “Versatile multicontact planning and control for legged loco-manipulation,” *Science Robotics*, p. eadg5014, 2023.
- [20] H. Ferrolho, V. Ivan, W. Merkt, I. Havoutis, and S. Vijayakumar, “Roloma: robust loco-manipulation for quadruped robots with arms,” *Auton. Robots*, vol. 47, no. 8, p. 1463–1481, Oct. 2023. [Online]. Available: <https://doi.org/10.1007/s10514-023-10146-0>
- [21] N. Yokoyama, A. W. Clegg, E. Undersander, S. Ha, D. Batra, and A. Rai, “Adaptive skill coordination for robotic mobile manipulation,” in *IEEE Robotics Autom. Lett. (RA-L)*. IEEE, 2024, pp. 779–786.
- [22] M. Liu, Z. Chen, X. Cheng, Y. Ji, R. Qiu, R. Yang, and X. Wang, “Visual whole-body control for legged loco-manipulation,” *CoRL*, 2024.
- [23] H. Ha, Y. Gao, Z. Fu, J. Tan, and S. Song, “UMI-on-legs: Making manipulation policies mobile with a manipulation-centric whole-body controller,” in *8th Annual Conference on Robot Learning*, 2024. [Online]. Available: <https://openreview.net/forum?id=3i7j8ZPnbm>
- [24] T. Portela, A. Cramariuc, M. Mittal, and M. Hutter, “Whole-body end-effector pose tracking,” *arXiv preprint arXiv:2409.16048*, 2024.
- [25] J. Schulman, F. Wolski, P. Dhariwal, A. Radford, and O. Klimov, “Proximal policy optimization algorithms,” *arXiv preprint arXiv:1707.06347*, 2017.
- [26] Z. Fu, A. Kumar, J. Malik, and D. Pathak, “Minimizing energy consumption leads to the emergence of gaits in legged robots,” in *Conference on Robot Learning*, 2021. [Online]. Available: <https://api.semanticscholar.org/CorpusID:237372201>
- [27] B. Sundaralingam, S. K. S. Hari, A. Fishman, C. Garrett, K. V. Wyk, V. Blukis, A. Millane, H. Oleynikova, A. Handa, F. Ramos, N. Ratliff, and D. Fox, “curobo: Parallelized collision-free minimum-jerk robot motion generation,” 2023.
- [28] L. Pinto, M. Andrychowicz, P. Welinder, W. Zaremba, and P. Abbeel, “Asymmetric actor critic for image-based robot learning,” in *Robotics: Science and Systems XIV, Carnegie Mellon University, Pittsburgh, Pennsylvania, USA, June 26-30, 2018*, H. Kress-Gazit, S. S. Srinivasa, T. Howard, and N. Atanasov, Eds., 2018. [Online]. Available: <http://www.roboticsproceedings.org/rss14/p08.html>
- [29] D.-A. Clevert, T. Unterthiner, and S. Hochreiter, “Fast and accurate deep network learning by exponential linear units (elus),” *arXiv: Learning*, 2015. [Online]. Available: <https://api.semanticscholar.org/CorpusID:5273326>